COMPDYN 2025
10th ECCOMAS Thematic Conference on
Computational Methods in Structural Dynamics and Earthquake Engineering
M. Papadrakakis, M. Fragiadakis (eds.)
Rhodes Island, Greece, 15-18 June 2025

THEORETICAL EVALUATION AND EXPERIMENTAL VALIDATION OF AN INNOVATIVE DYNAMIC ANALYSIS METHOD FOR COMBINED STRUCTURES WITH TUNED MASS DAMPERS

John Bellos[1], Vasileios C. Kamperidis[1], Salomi Papamichael[1], and Anthos Ioannou[1]

[1] Neapolis University Pafos

Danais Avenue 2, Paphos, 8042, Cyprus

{j.bellos, v.kamperidis, s.papamichael, a.ioannou}@nup.ac.cy

Abstract

Tuned Mass Dampers (TMDs) is an effective way for mitigating vibrations and sways in engineering structures under lateral actions, such as strong winds. Thus, TMDs can enhance safety and reduce design structural demands. The design approach for systems with TMDs is crucial for both the accuracy and efficiency of their design. However, the current design approaches have either some practicality disadvantages, or cannot provide accurate and effective solutions in all cases. To this end, Bellos et al. [2] recently proposed a robust and versatile hybrid analytical-numerical design method that can address these shortcomings. The method accounts for distributed parameters and non-proportional damping, and can apply to non-conservative systems under all types of external actions. Yet, this method has not experimentally been validated. The main objectives of this work are to experimentally validate the aforementioned method, demonstrate its extended applicability, and provide a handy and accurate means for engineers to design systems with TMDs accurately and efficiently. The latter is realized by providing design charts, in lieu of using heavy numerical simulations, or other impractical and oversimplified methods. To achieve its objectives, the work utilizes a scaled down, two-storey building experimental setup with and without a TMD at its top. Parametric analyses are then performed for varying values of characteristic design parameters of the investigated system. The experiments show a good agreement with the theoretical results, thus validating the accuracy of the method. The results demonstrate the effectiveness of the method in reducing critical performance indices of the structure under winds by up to about 90% for realistic values of the TMB design properties. The work lays the foundation for implementing the method in complex structures with multiples TMDs in random positions.

Keywords: Tuned Mass Dampers (TMDs); Combined Dynamic Systems; Metastructures; Non-classically Damped Systems; Non-proportional Damping; Nonlinear Modal Analysis.

1 INTRODUCTION

Structural engineering has long relied on vibration control mechanisms to improve building performance under lateral loads, particularly in high-rise buildings and long-span structures. Among the most widely used solutions, Tuned Mass Dampers (TMDs) have demonstrated remarkable efficiency in controlling excessive displacements and accelerations by transferring vibrational energy from the primary structure to secondary mass systems [3, 4]. TMDs have been successfully implemented in various landmark structures. Currently, the largest globally TMD is in Taipei 101, where the TMD action can reduce wind-induced accelerations significantly [5, 6]. Other real building examples include the Citigroup Center in New York, USA (initially named as "Citicorp Center", while now is officially known as "601 Lexington Avenue") [7], and the Shanghai Centre Tower (SHT) [6].

The design of systems with TMDs involves the fine-tuning of the design properties of TMD. This fine-tuning process has been the main focus of many researchers throughout the years [8]. Commencing from the seminal work by Den Hartog et al. [4] and moving to improvements of the method, such as those of Warburton and Ayorinde [9], the design of TMD-equipped structures has gained particular interest for researchers. It typically involves the derivation of optimal mass, damping, and stiffness parameters for the TMD using frequency-based tuning approaches [8, 10], Modal Analysis-based techniques for TMD placement and design [8, 11, 12] and Energy-based TMD optimization approaches [4, 13, 14]. More modern applications for refining TMD configurations, include numerical optimization methods [15, 16], involving Artificial Neural Networks (ANN) [17, 18], Machine Learning techniques [19, 20], Genetic Algorithms (GAs) [21, 22] and Particle Swarm Optimization (PSO) [23].

Despite the success of classical TMD design methodologies, challenges persist in accurately modeling structures with non-proportional damping and complex dynamic interactions (e.g., complex modes of vibration). In addition, more modern techniques, involve dependency on heavy computational tools and thus associate with computational complexity [21], while still cannot fully address some of the shortcomings of the classical approaches. To address these issues, Bellos et al. [2] proposed a novel hybrid analytical-numerical framework, which extends traditional methodologies by incorporating non-proportional damping effects, random plasticity distribution, and a generalized modal decomposition approach. However, while theoretical validation of this method has been extensively conducted [1, 2], no experimental studies have yet confirmed its applicability in real-world structures.

The primary objective of this research is to provide an experimental validation of the Bellos et al. [2] methodology, which will henceforth be called innovative method [2], through a scaled-down two-storey building prototype equipped with a TMD. Secondly, the work proposes a design chart (nomograph) for the accurate tuning of systems with TMDs, otherwise called combined structures with TMDs. Utilizing such design charts, a Structural Engineer is given the option to design System with TMDs without the need of a dedicated software. In fact, the model proposed in [2] allows for the placement of multiple TMD, in various positions of the building, as utilizing more than one TMD has been shown to be more effective than using a single TMD [24]. The work also explores the effectiveness of the method in mitigating wind-induced vibrations and demonstrates the potential of the extended applicability of the method in structures with multiple TMDs.

2 THEORETICAL MODEL

The theoretical basis for this study follows the analytical framework established in [2], where the authors used an Euler-Bernoulli beam model with viscously damped oscillators attached to represent the actual structure. The present study adapts this formulation by considering a vertical Euler-Bernoulli beam to model a building structure, where the building's lateral sway behavior is approximated as that of a distributed parameter system. The vertical beam model is fixed at its lower end, while having multiple oscillators attached to it (see Figure 1).

The Euler-Bernoulli beam model is a well-established approximation for representing the behavior of slender, flexural-dominant structures under dynamic loading [25]. It is particularly useful when modeling tall buildings subjected to lateral wind forces, where the lateral displacements and rotations can be assumed to follow small-strain linear elasticity principles. In such cases, the building behaves as a continuous, distributed-parameter system, and its response can be effectively captured through modal decomposition techniques [26]. The equivalency of a high-rise building to an Euler-Bernoulli beam is especially valid in cases where:

a) The structure exhibits dominant flexural behavior, meaning that shear deformations are negligible compared to bending deformations [27].
b) The structure has a regular geometry and consistent mass and stiffness distribution over its height [28].
c) The external excitation, such as wind loads, acts predominantly as a distributed lateral force rather than a point load [29].

Structures as such, comprising a main structure and oscillator appendages, in our case TMDs, are known as combined dynamic systems or metastructures (see configuration in Figure 1).

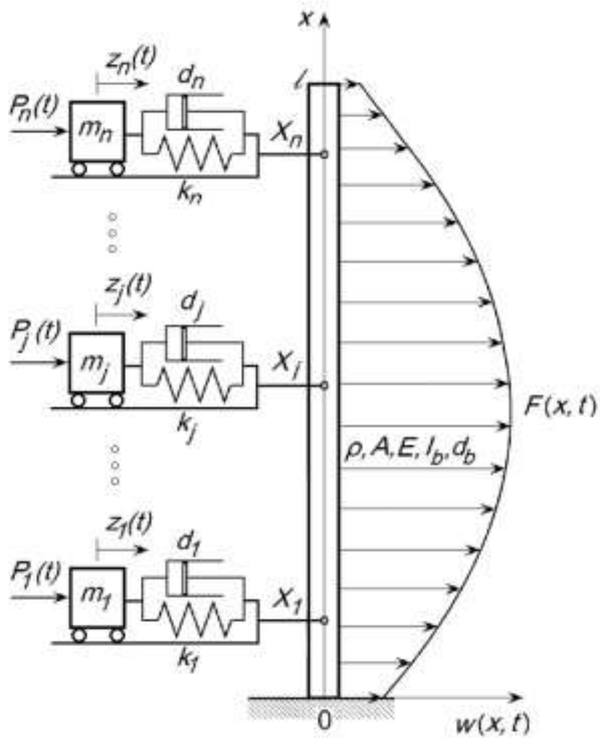

Figure 1: The vertical Euler-Bernoulli beam with oscillator appendages (TMDs) to model a combined building structure with TMDs.

In the above figure, t is the time variable; l is the height of the main structure (beam length); x is vertical location on the main structure; $w(x,t)$ is the dynamic displacement along the main structure (beam deflection); $F(x,t)$ is the distributed external excitation on the main structure, i.e. in our case could represent wind load. The index '*n*' denotes the number of oscillators of the combined system(in our case number of TMDs); m_j, d_j and k_j represent the mass, damping and stiffness properties of the j[th] oscillator, respectively; $z_j(t)$ is the dynamic displacement of the j[th] oscillator; $P_j(t)$ is the external force imposed at the j^{th} oscillator at the location X_j via the *Dirac Delta* function $\delta(x-X_j)$.

The boundary conditions of the problem are determined as per the following equation:

$$w(0,t)=\left.\frac{\partial w(x,t)}{\partial x}\right|_{x=0}=0, \quad \text{for} \quad t\geq 0, \tag{1}$$

while the initial conditions are considered homogeneous:

$$w(x,0)=\left.\frac{\partial w(x,t)}{\partial t}\right|_{t=0}=0, \quad \text{for} \quad 0\leq x\leq l. \tag{2}$$

As it can be understood, combined dynamic systems like the above can represent anything from a horizontal structure, such as a bridge with dampers positioned in key locations, up to a normal building structure, where the dampers can be placed anywhere along its height. The governing equation of motion, for all these structures will remain the one next, derived in [2]:

$$\rho\cdot A\cdot\frac{\partial^2 w(x,t)}{\partial t^2}+d_b\cdot\frac{\partial w(x,t)}{\partial t}+E\cdot I_b\cdot\frac{\partial^4 w(x,t)}{\partial x^4}=\sum_{j=1}^{n}F_j(t)\cdot\delta(x-X_j)+F(x,t), \quad 0\leq x\leq l, \quad t\geq 0, \tag{3}$$

Here ρ and E are the density and modulus of Elasticity of its material, respectively; A and I_b are the cross-sectional area and moment of inertia of the equivalent beam, respectively; d_b is its distributed damping; $F_j(t)$ are the reaction forces exerted by the oscillators to the main structure. These latter forces are given as per the relationship:

$$F_j(t)=d_j\cdot\left[\dot{z}_j(t)-\frac{\partial w(X_j,t)}{\partial t}\right]+k_j\cdot\left[z_j(t)-w(X_j,t)\right]=-m_j\cdot\ddot{z}_j(t)+P_j(t), \quad j=1,2,...,n. \tag{4}$$

It must be noted that, in our case, $P_j(t)=0,\ j=1,2,...,n$, since no external forces or controls are considered to be imposed on our TMDs.

Next, the problem can be made dimensionless by normalizing to space, time and mass, through the normalization parameters, l, τ, μ, respectively. These normalization parameters are defined as:

$$\tau=l^2\cdot\sqrt{(\rho\cdot\mathrm{A})/(\mathrm{E}\cdot\mathrm{I_b})}, \qquad \mu=\rho\cdot\mathrm{A}\cdot l. \tag{5}$$

Considering Eqns. (5), the problem can now be written in terms of its dimensionless forms, expressed through the capped forms of their initial parameters, as per the following formulas:

$$\begin{aligned}
&\hat{t}=t/\tau, \quad \hat{\omega}_i=\omega_i\cdot\tau, \quad \hat{\Omega}_j=\Omega_j\cdot\tau, \quad \hat{X}_j=X_j/l, \quad \hat{x}=x/l,\\
&\hat{m}_j=m_j/\mu, \quad \hat{k}_j=k_j\cdot\tau^2/\mu, \quad \hat{d}_j=d_j/m_j\cdot\tau, \quad \hat{d}_b=d_b\cdot l\cdot\tau/\mu,\\
&w(\hat{x},\hat{t})=w(x,t)/l, \quad z_j(\hat{t})=z_j(t)/l, \quad \delta(\hat{x}-\hat{X}_j)=\delta(x-X_j)/l,\\
&F(\hat{x},\hat{t})=F(x,t)\cdot\tau^2/\mu, \quad P_j(\hat{t})=P_j(t)\cdot\tau^2/(\mu\cdot l), \quad F_j(\hat{t})=F_j(t)\cdot\tau^2/(\mu\cdot l).
\end{aligned} \tag{6}$$

where $\Omega_j=\sqrt{k_j/m_j}$ is the undamped natural frequency of the j^{th} oscillator, in our case of the j^{th} TMD, and ω_i and $\Phi_i(x)$ are respectively the natural frequency and eigenfunction of the i^{th} mode of the undamped structure. Note that the values of $\omega_\imath$ and $\Phi_i(x)$ are derived through nonlinear modal analysis, using Eqns. (20) and (26) presented in [2].

Consequently, Eqns. (3) and (4) are expressed in dimensionless form as

$$\frac{\partial^2 w(\hat{x},\hat{t})}{\partial \hat{t}^2}+\hat{d}_b\cdot\frac{\partial w(\hat{x},\hat{t})}{\partial \hat{t}}+\frac{\partial^4 w(\hat{x},\hat{t})}{\partial \hat{x}^4}=\sum_{j=1}^{n}F_j(\hat{t})\cdot\delta(\hat{x}-\hat{X}_j)+F(\hat{x},\hat{t}),\quad 0\le\hat{x}\le 1,\quad \hat{t}\ge 0, \tag{7}$$

and

$$F_j(\hat{t})=\hat{d}_j\cdot\left[\dot{z}_j(\hat{t})-\frac{\partial w(\hat{X}_j,\hat{t})}{\partial \hat{t}}\right]+\hat{k}_j\cdot\left[z_j(\hat{t})-w(\hat{X}_j,\hat{t})\right]=-\hat{m}_j\cdot\ddot{z}_j(\hat{t})+P_j(\hat{t}),\qquad j=1,2,\ldots,n. \tag{8}$$

The correlation of the above Eqns. (7) and (8) with Eqns. (1) and (7) presented in [2], respectively (not repeated here for brevity), representing the general model of combined dynamic systems, yields the operators L_1 and L_2, as per the following relationships:

$$L_1=\hat{d}_b\cdot I \qquad \text{and} \qquad L_2=\frac{\partial^4}{\partial \hat{x}^4}, \tag{9}$$

where I is the identity operator. These two operators are two linear, self-adjoint, positive definite differential operators [30], which represent damping and stiffness characteristics of the main structure, respectively, and which comprise partial derivatives with respect to the spatial variable x. Moreover, each of the differential operators of Eq. (9) is defined in a domain with continuous fourth order spatial derivatives, expressed as R=L^4(0,1). Utilizing Eq. (9), one could attain the introduction of material nonlinearity into the model.

Finally, the couple problem can be written in its dimensionless form, and in its natural coordinates as:

$$\begin{aligned}&\ddot{a}_i(\hat{t})+\sum_{k=1}^{\infty}\left\{\hat{d}_b\cdot\delta_{ik}+\sum_{j=1}^{n}\hat{m}_j\cdot\left(\hat{d}_j\cdot\frac{\hat{\omega}_i^2\cdot\hat{\omega}_k^2}{\hat{\Omega}_j^4}-\hat{d}_b\right)\cdot A_{ji}\cdot A_{jk}\cdot\Phi_i(\hat{X}_j)\cdot\Phi_k(\hat{X}_j)\right\}\cdot\dot{a}_k(\hat{t})+\\&+\hat{\omega}_i^2\cdot a_i(\hat{t})=\int_0^1 F(\hat{x},\hat{t})\cdot\Phi_i(\hat{x})\cdot d\hat{x}+\sum_{j=1}^{n}A_{ji}\cdot P_j(\hat{t})\cdot\Phi_i(\hat{X}_j),\qquad i=1,2,\ldots,\infty,\end{aligned} \tag{10}$$

where $a_i(t)$ is the i^{th} modal displacement, δ_{ik} is the kronecker delta, and $A_{ji}=\Omega_j^2\big/\left(\Omega_j^2-\omega_i^2\right)$ is i^{th} modal magnification factor of the j^{th} oscillator.

3 PROTOTYPE BUILDING AND EXPERIMENTAL SETUP

3.1 Design cases

For the validation of the theoretical methodology presented in [2], a two-storey scaled-down building model was utilized. The model comprised a proprietary experimental setup from Quanser [31]. The model in question represented a moment-resisting frame (MRF). For the scope of this research, two design configurations considered for comparison, notably a system with a TMD versus one without TMD. The two systems are shown in Figure 2. The system at the left (Figure 2(a)), i.e. the one without the TMD, served as the benchmark design case of this work. The names of the levels of the investigated prototype model are shown in Figure 2(a).

In this work, a single TMD device (see Figure 2(c)) is fixed on the top of Level 2 of the experimental setup (see Figure 2(b)). This is because the dominant mode of vibration of such a structure is usually the first mode. Therefore, its maximum value is meant to be at, or close to, the location where the maximum storey displacement is anticipated, i.e. near the top of the building, as per previous relevant research [32, 33, 34].

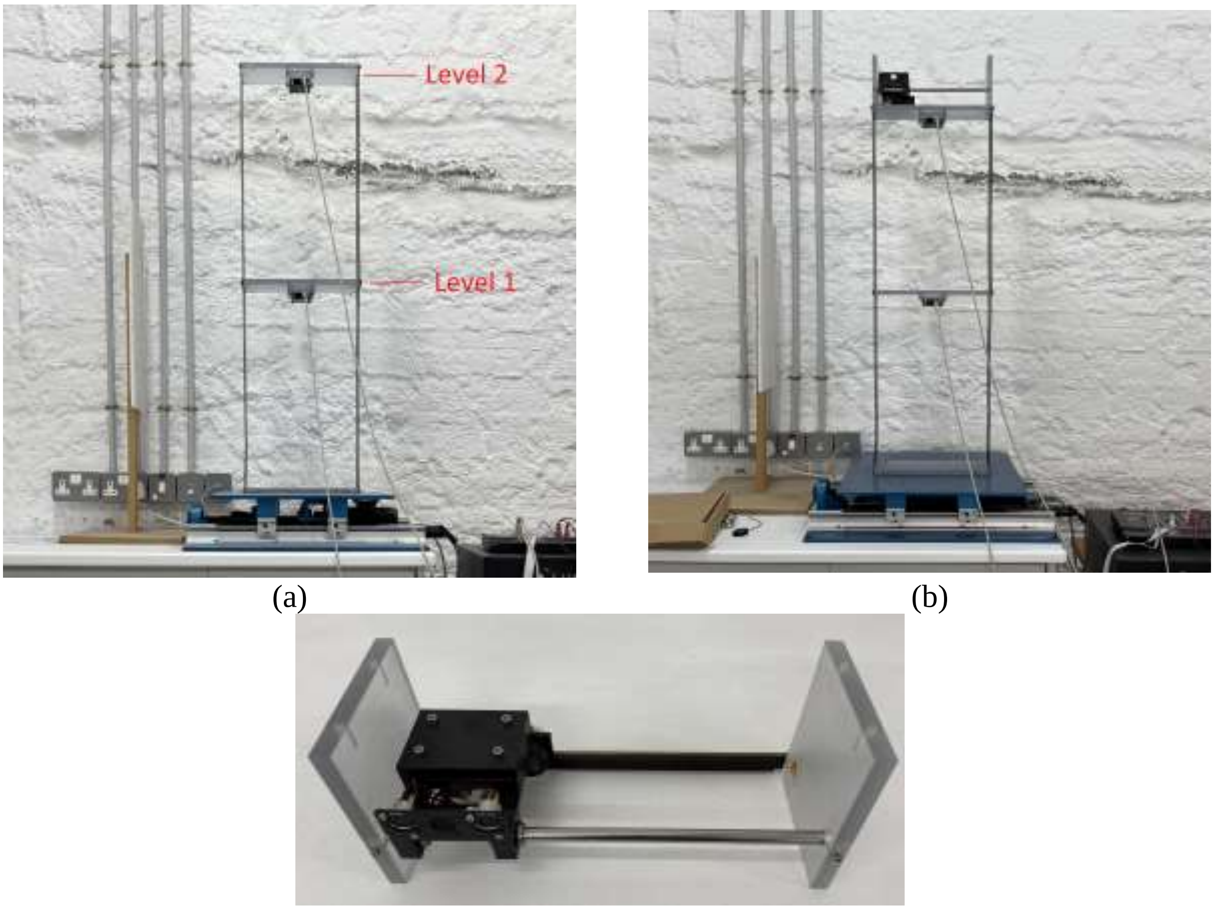

(a) (b)

(c)

Figure 2: The experimental device: (a) without TMD (b) with TMD (c) The TMD device itself (placed at the top of the device in (b)).

4 NUMERICAL MODELLING AND ANALYSIS

4.1 Numerical Modeling

The experimental setup was modelled as an equivalent Euler-Bernoulli beam, on the grounds of the theory presented in Section 2. The loading utilized for this research is a wind load of sinusoidal form. The distributed load is applied to the model through $F(x, t)$ of Eq. (1), described above. The performance criterion used for assessing the performance of the investigated experimental setup, as well as for the hybrid model in [2], is the peak displacement (or peak drift) of the equivalent beam, as this is one of the classical performance indicators for such systems [13].

In the first place, analyses conducted, utilizing the theoretical model presented in [2] for the equivalent beam comprising two flexible metal strips rigidly connected at Level 1 and Level 2. Two design cases of the beam examined: one without TMD and one with TMD. In both cases, the beam geometrical and material properties were the following:

Total length: l = 0.976 (m);
Mass Density: ρ = 2700 (kg/m^3);
Cross-sectional Area: A = 4.18*10^{-4} (m^2);
Modulus of Elasticity: E = 6.8*10^{10} (N/m);
Moment of Inertia: I_b = 4.65*10^{-10} (m^4);
Damping coefficient: d_b = 1.5 (Kg/sec/m).

For the two investigated cases, the rigid connectors at the two levels were modelled as lumped mass oscillators of high stiffness and damping values. The properties of the lumped mass oscillators along with the properties of the TMD are shown in Table 1.

Properties of the lumped mass oscillators	Case without TMD		Case with TMD		
	Level 1	Level 2	Level 1	Level 2	TMD
Position (m)	0.5·*l**	1.0·*l*	0.5·*l*	1.0·*l*	1.0·*l*
Mass (kg)	0.635	0.635	0.635	1.435	0.520
Stiffness (N/m)	500.0	500.0	500.0	500.0	0.0
Damping (kg/sec)	100.0	100.0	100.0	100.0	0.5

* *l* refers to the total height of the building, which in this case represents the total height of the device

Table 1: Properties of the lumped mass oscillators for the investigated two design cases.

In our case, the normalization parameters resulted from Eqns. (5) are:

$l = 0.976$ (m), $\tau = 0.180$ (sec), $\mu = 1.102$ (Kg).

4.2 Numerical Analyses

In the first place, this work investigated the importance of considering modal coupling, as per the work in [1]. To this end, the first six modes of vibration of the structure with and that without the TMD were determined.

The misleading errors of neglecting the modal coupling in the response of such a combined structure are inferred in Figure 3.

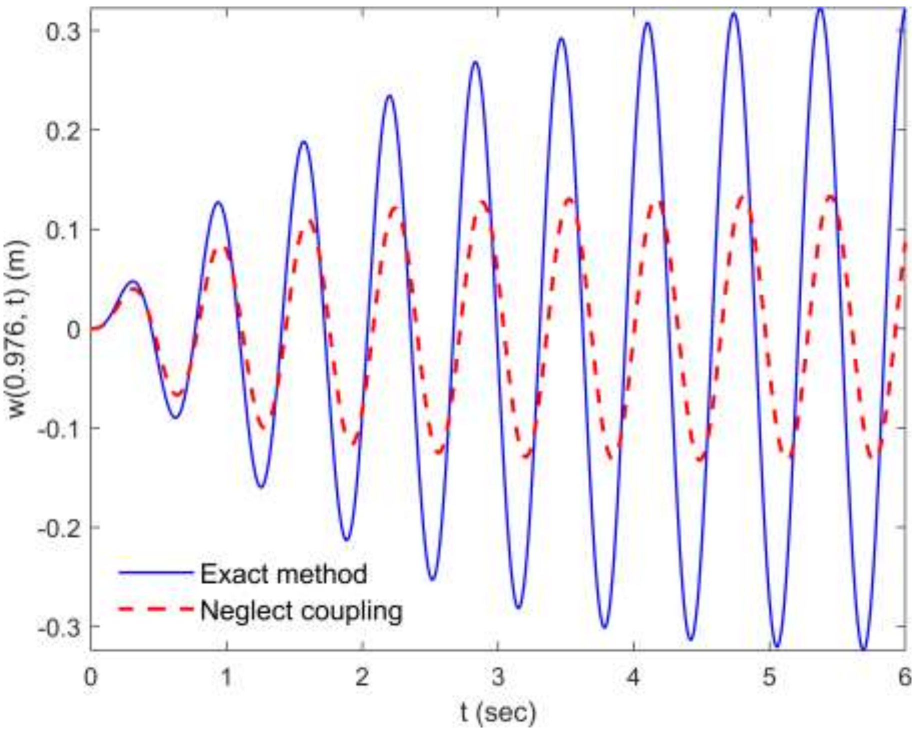

Figure 3: Dynamic response at the top of the 2-storey model with TMD at the top, for the cases of considering or neglecting modal coupling and for excitation of the first mode of the main structure.

Considering modal coupling, for the two cases of the beams (as per Section 3.1), the six first modes of vibrations derived using nonlinear modal analysis, as per [2]. From these modes, Table 2 lists their correspondent frequencies.

Mode	Case without TMD		Case with TMD	
	ω (rad/sec)	f (Hz)	ω (rad/sec)	f (Hz)
1	9.81	1.56	7.13	1.13
2	26.39	4.20	25.50	4.06
3	53.66	8.54	50.89	8.10
4	133.96	21.32	133.77	21.29
5	345.58	55.00	345.51	54.99
6	673.87	107.25	673.87	107.25

Table 2: First six natural frequencies for the two design cases.

As it can be seen from the values of Table 2, the effect of the TMD subsides while moving up to higher modes of vibrations; this is demonstrated by the difference in the frequency response of the structure with and without the TMD, which gradually decreases, ending up to zeroing when reaching the sixth mode. This is grounded on the fact that we have adjusted our TMD to have damping properties that generate modal coupling in the lower modes of our main structure, thus shifting the respective natural frequencies of the combined structure away from resonance while absorbing maximum energy for the respective modes of vibration.

The mode shapes of the first six modes of vibration of the system can be seen in Figure 4. Using the methodology presented in [2], a continuous model is obtained for our structure with an infinite number of degrees of freedom (DOFs) and, therefore, one can easily determine the appropriate number of truncated mode shapes for the real structure. As such, i.e. by requiring additional mode shapes, the dynamic response of the corresponding actual structure is calculated more accurately compared to the response approximated by other methods, such as lumped parameter approximations.

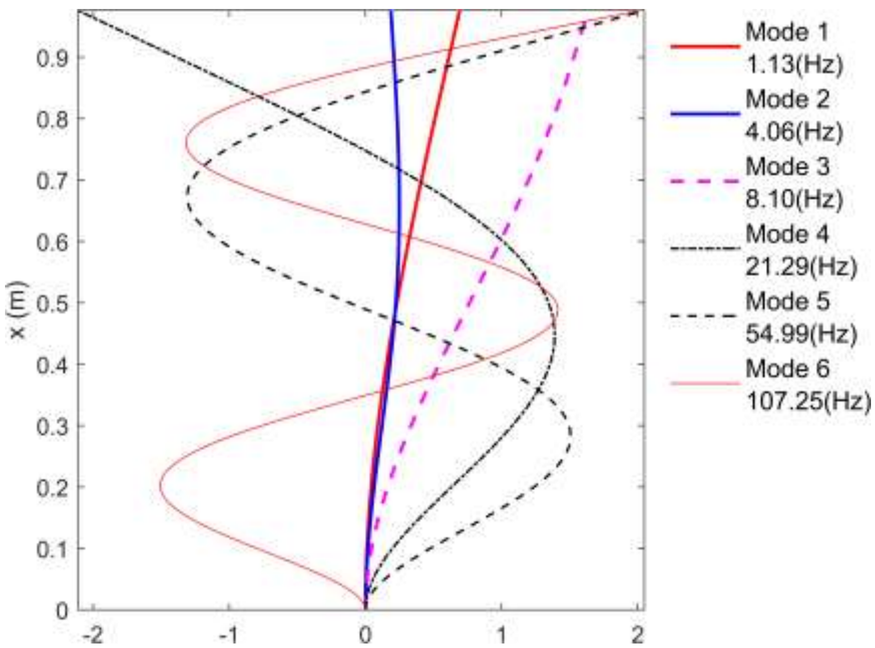

Figure 4: The six mode shapes of the combined structure, as derived using the innovative method [2].

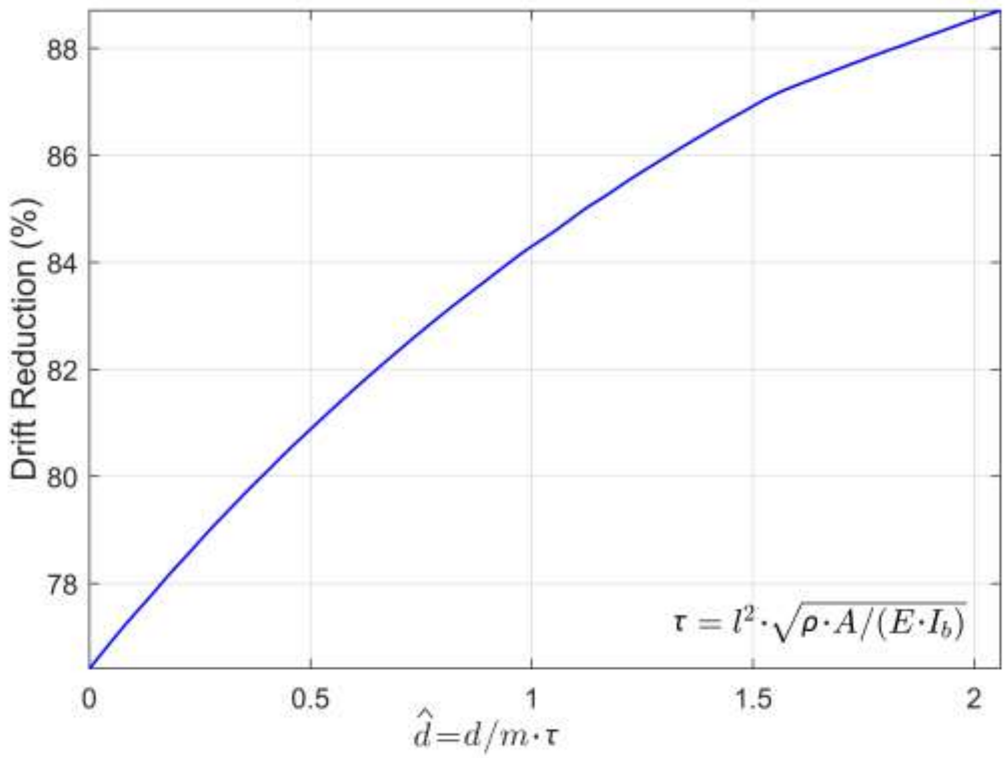

Figure 5: Drift reduction percentage versus normalized damping $\hat{d}$ of a springless TMD attached to the top of the 2-storey model, for excitation of the first mode of the main structure.

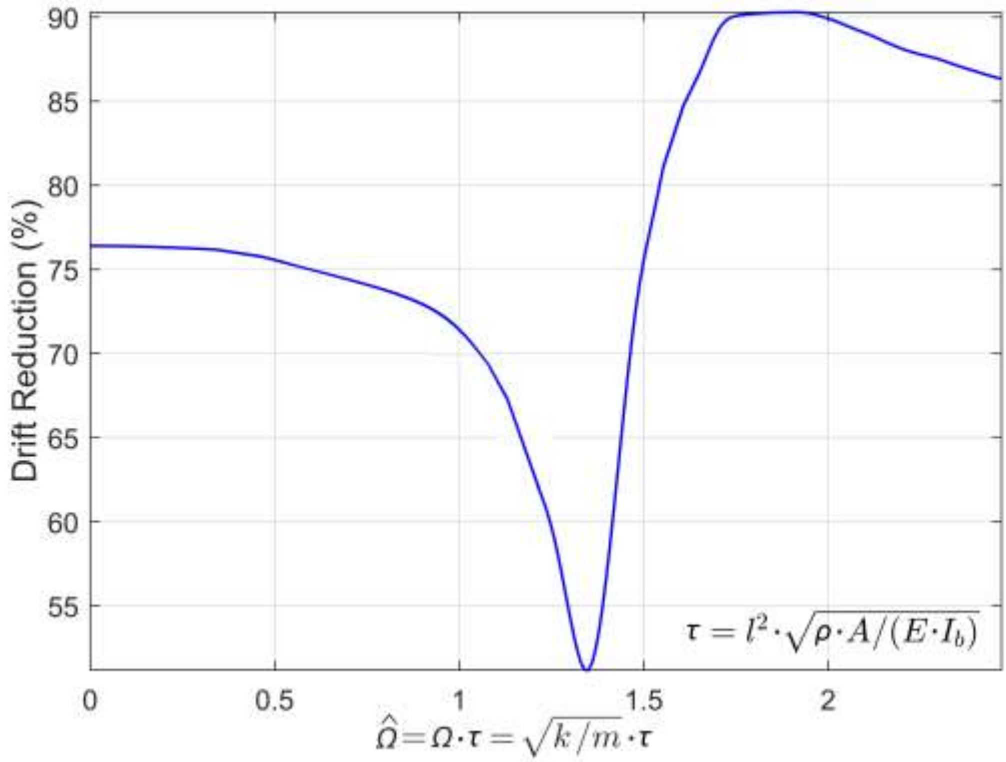

Figure 6: Drift reduction percentage versus normalized natural frequency $\hat{\Omega}$ of an undamped TMD attached to the top of the 2-storey model, for excitation of the first mode of the main structure.

This work numerically investigates the effectiveness of the TMD on the dynamic response of the 2-storey model, under the scenario of an externally applied sinusoidal wind load exciting the first mode of the main structure. Figures 5 and 6 show how the peak drift is affected by properties of a TMD attached to the top of the 2-storey model. In fact, they present the drift reduction percentage versus the normalized damping $\hat{d}$ of a springless TMD and versus the normalized natural frequency $\hat{\Omega}=\Omega\cdot\tau$ of an undamped TMD, respectively. Notice in Figure 6, for example, that the region $1.0\leq\hat{\Omega}\leq1.5$ or the respective region $5.55\leq\Omega\leq8.33$ (in rad/sec) should be avoided.

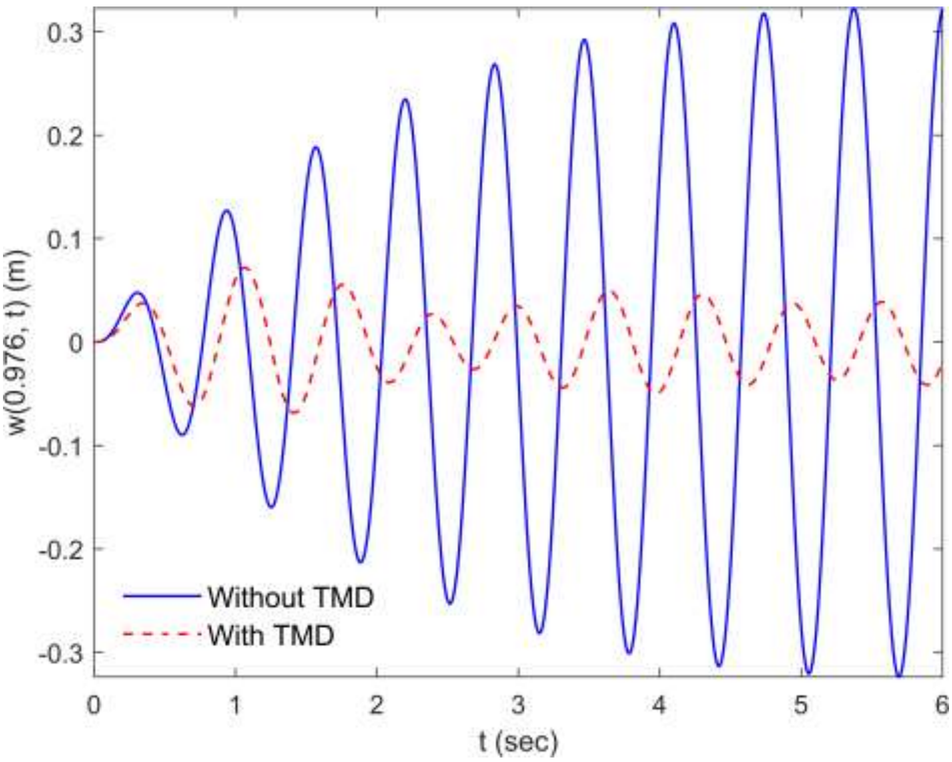

Figure 7: Dynamic response at the top of the 2-storey model without and with TMD at the top, for excitation for excitation of the first mode of the main structure.

Figure 7 shows a comparison of the dynamic responses between the two design cases, when exciting the first mode of the 2-storey model. The response shown on the graph refers to the horizontal displacement of the top level of the investigated 2-storey model. As it can be seen from the graph, utilizing the TMD, which has been designed as per the methodology in [2], can drastically reduce the maximum drift of the modelled building. More specifically, for the given design, the maximum drift reduction achieved is of the order of 83.2%. However, and as it will be shown next (Section 4.3), greater reductions can also be achieved.

4.3 Design Charts

In this section, this work constructs and provides a useful tool for designing effectively, and accurately, the main design properties of a combined structure with TMD. This is realized through a proposed design chart (Nomograph), which is shown in Figure 8. It is highlighted that the design chart has been constructed to provide effective TMD designs for a wide range of realistic and attainable values of TMD design attributes. Note that the design chart is unitless to be more practical.

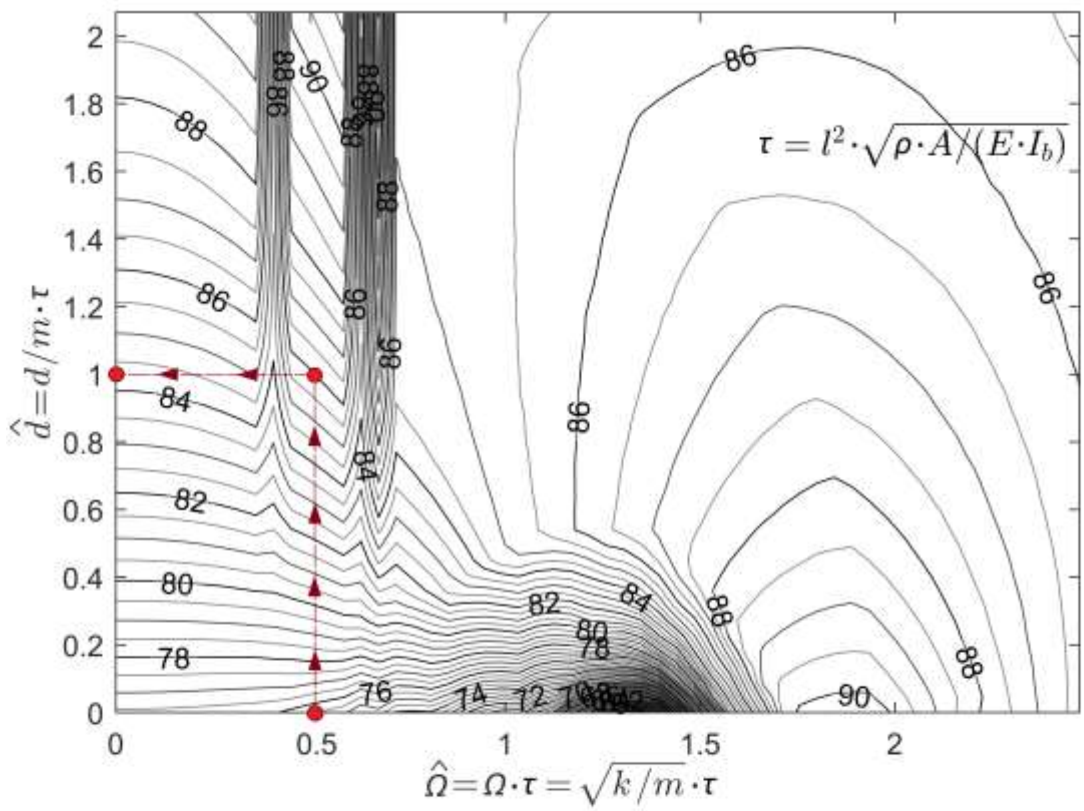

Figure 8: Drift reduction percentage versus normalized TMD properties, after applying a TMD at the top, for excitation of the first mode of the main structure.

As it can be observed from the above design chart, there are two regions of particular interest: one that should be avoided, and one that it should be sought after. For the first one, the designer should avoid the region $1.0 \le \hat{\Omega} \le 1.5$ and $\hat{d} \le 0.2$. This is identified here as the "avoidable" region of the design chart. In this region the attached TMD fails to shift the respective natural frequencies of the combined structure away from resonance. On the other end of the spectrum, an optimum design can be achieved in the region $0.4 \le \hat{\Omega} \le 0.6$ and $\hat{d} \ge 0.8$, where, obviously, the main structure's resonates and applying a TMD at the top achieves a significant drift reduction. This is identified here as a "targeted" region of the design chart.

4.4 Design Example

To demonstrate the practicality of the design chart of Figure 8, let us assume that for our 2-storey model we apply a TMD at the top with a spring stiffness k=5 (N/m).

In Figure 8, we choose a normalized natural frequency $\hat{\Omega}=0.5$ while we seek a drift reduction percentage of approximately 86%. Then, the design chart provides a normalized damping $\hat{d}=1.0$. The design parameters of the TMD are obtained as:

$$\hat{\Omega}=\Omega\cdot\tau \Rightarrow \Omega=\hat{\Omega}/\tau \Rightarrow \Omega=0.5/0.18 \Rightarrow \Omega=2.78 \text{ (rad/sec)},$$

$$\Omega=\sqrt{k/m} \Rightarrow m=k/\Omega^2=5/2.78^2 \Rightarrow m=0.647 \text{ (Kg)},$$

$$\hat{d}=d/m\cdot\tau \Rightarrow d=\hat{d}\cdot m/\tau \Rightarrow d=1.0\times 0.647/0.18 \Rightarrow d=3.59 \text{ (Kg/sec)}.$$

The TMD device with the above properties will provide a drift reduction percentage of 86% for the combined 2-storey model.

5 EXPERIMENTAL VALIDATION

5.1 Experimental Results

The work aimed to validate the accuracy of the innovative method [2]. To this end, the first two modes of vibration numerically investigated in Table 2, were also replicated in the labs, as per the setup described in Section 3.

Table 3 compares the frequencies of the first two modes derived experimentally from the lab experiments with those of Table 2 derived theoretically.

Case without TMD				Case with TMD			
Theoretical		Experimental		Theoretical		Experimental	
ω (rad/sec)	f (Hz)	ω (rad/sec)	f (Hz)	ω (rad/sec)	f (Hz)	ω (rad/sec)	f (Hz)
9.81	1.56	9.68	1.54	7.13	1.13	7.04	1.12
26.39	4.20	26.52	4.22	25.50	4.06	21.99	3.5

Table 3: Comparison of the theoretical and experimental results of the two first modes for the two design cases.

As observed from Table 3, the theoretical derived values by using the methodology proposed in [2] are in a good agreement with the corresponding experimentally derived values.

6 SUMMARY AND CONCLUSIONS

Based on the findings of this work, the following conclusions are drawn:

1. A hybrid analytical-numerical design method [2] has been experimentally validated for low-rise construction, and for conventional MRF systems.
2. The work shows that considering modal coupling is necessary in predicting more accurately the response of a combined structure.
3. A handy, accurate and effective design tool, namely, a design chart (nomograph), has been proposed in this work for Structural Engineers to use to design structural systems with TMD, without the need to resort to complex mathematical design processes.
4. The design chart identifies a “targeted” and an “avoidable” region for the design of metastructures with TMDs. For the “targeted” region, performance improvement up to 90% can be achieved, for a wide but realistic and attainable range of the design properties of the TMDs.
5. Selecting an appropriate method, such as the innovative method [2], can have a significant effect on the level of performance improvement that can be achieved for a structure equipped with TMD.

Future work aims to:

a) Adjust Eq. (51) of the methodology presented in [2] to introduce lumped plasticity in the model.
b) Use the same experimental device to vary the number of TMDs and, thus, extend the experimental findings relevant to this work.
c) Extend the findings of this work to investigate the effect of higher mode effects by constructing finite element method models that represent taller buildings with TMD in software such as OpenSees [35].
d) Investigate cases of combined seismic and wind loads.

e) Effectively combine additional performance indices to design metastructures with TMDs more holistically, construct the design charts for the additional performance indices and propose methods for combining the design charts.
f) Introduce additional design charts for new performance indices and propose a new method for combining these with the existing ones in this work; this aims to a more effective design of metastructures.
g) Further extend the applicability of the current innovative approach of [2] by introducing an Automated TMD Placement Optimization Technique, by using, for example, Machine Learning (ML).

REFERENCES

[1] J. Bellos, D.J. Inman, N. Bakas, Nature of coupling in non-conservative distributed parameter systems attached to external damping sources, Mathematics and Mechanics of Solids, 25(7), 1367–1383, 2017.

[2] J. Bellos, D.J. Inman, Modal analysis of non-conservative combined dynamic systems, Journal of Vibration and Acoustics, 144(1), 011008, 2022. https://doi.org/10.1115/1.4052819.

[3] H. Frahm, Device for damping vibrations of bodies, U.S. Patent 989,958, 1909.

[4] J.P. Den Hartog, Mechanical Vibrations, Dover Publications, Mineola, NY, 1934, pp. 93–106.

[5] K.C. Chen, J.H. Wang, B.S. Huang, C.C. Liu, W.G. Huang, Vibrations of the TAIPEI 101 skyscraper induced by Typhoon Fanapi in 2010, Terrestrial, Atmospheric and Oceanic Sciences, 24, 1–10, 2013. https://doi.org/10.3319/TAO.2012.09.17.01(T).

[6] X. Lu, Q. Zhang, D. Weng, Z. Zhou, S. Wang, S.A. Mahin, S. Ding, F. Qian, Improving performance of a super tall building using a new eddy-current tuned mass damper, Structural Control and Health Monitoring, 24, e1882, 2017. https://doi.org/10.1002/stc.1882.

[7] W. LeMessurier, The fifty-nine-story crisis: a lesson in professional behavior, National Academy of Engineering, 1995. [Online], Available at: https://onlineethics.org/cases/engineers-and-scientists-behaving-well/william-lemessurier-fifty-nine-story-crisis-lesson

[8] R. Rana, T.T. Soong, Parametric study and simplified design of tuned mass dampers, Engineering Structures, 20(3), 193–204, 1998. https://doi.org/10.1016/S0141-0296(97)00078-3.

[9] G.B. Warburton, E.O. Ayorinde, Optimum absorber parameters for simple systems, Earthquake Engineering and Structural Dynamics, 8, 197–217, 1980. https://doi.org/10.1002/eqe.4290080302.

[10] T.T. Soong, G.F. Dargush, Passive Energy Dissipation in Structural Engineering, John Wiley & Sons, Chichester, 1997.

[11] G.B. Warburton, Optimum absorber parameters for various combinations of response and excitation parameters, Earthquake Engineering and Structural Dynamics, 10(3), 381–401, 1982. https://doi.org/10.1002/eqe.4290100304.

[12] V.M. Thakur, O.R. Jaiswal, Optimum parameters of variant tuned mass damper using equal eigenvalue criterion, Earthquake Engineering and Structural Dynamics, 52, 2852–2860, 2023. https://doi.org/10.1002/eqe.3884.

[13] R. Greco, G.C. Marano, Optimum design of Tuned Mass Dampers by displacement and energy perspectives, Soil Dynamics and Earthquake Engineering, 49, 243–253, 2013, Available at: https://doi.org/10.1016/j.soildyn.2013.02.013

[14] M.R. Shayesteh Bilondi, H. Yazdani, M. Khatibinia, Seismic energy dissipation-based optimum design of tuned mass dampers, Structural and Multidisciplinary Optimization, 58, 2517–2531, 2018. https://doi.org/10.1007/s00158-018-2033-0.

[15] J. Štěpánek, J. Máca, Optimization of tuned mass dampers – minimization of potential energy of elastic deformation, Advances in Engineering Software, 197, 103756, 2024. https://doi.org/10.1016/j.advengsoft.2024.103756.

[16] SV Kontomaris, I Mazi, G Chliveros, A Malamou, Generic numerical and analytical methods for solving nonlinear oscillators, Physica Scripta 99 (2), 2024, 025231.

[17] M. Ramezani, A. Bathaei, A.K. Ghorbani-Tanha, Application of artificial neural networks in optimal tuning of tuned mass dampers implemented in high-rise buildings subjected to wind load, Earthquake Engineering and Engineering Vibration, 17(4), 903–915, 2018. https://doi.org/10.1007/s11803-018-0483-4.

[18] C. Söyleyici, H.Ö. Ünver, A physics-informed deep neural network based beam vibration framework for simulation and parameter identification, Engineering Applications of Artificial Intelligence, 141, 109804, 2025. https://doi.org/10.1016/j.engappai.2024.109804.

[19] S. Etedali, N. Mollayi, Cuckoo search-based least squares support vector machine models for optimum tuning of tuned mass dampers, International Journal of Structural Stability and Dynamics, 18(2), 1850028, 2017. https://doi.org/10.1142/s0219455418500281.

[20] B. Fu, X.H. Liu, J. Chen, Machine learning-based hybrid optimization method for tuned mass damper considering seismic soil-structure interaction, Journal of Earthquake Engineering, 1–22, 2024. https://doi.org/10.1080/13632469.2024.2334824.

[21] P. Wielgos, R. Geryło, Optimization of multiple tuned mass damper (MTMD) parameters for a primary system reduced to a single degree of freedom (SDOF) through the modal approach, Applied Sciences, 11(4), 1389, 2021. https://doi.org/10.3390/app11041389.

[22] H.Q. Cao, N.A. Tran, Multi-objective optimal design of double tuned mass dampers for structural vibration control, Archive of Applied Mechanics, 93, 2129–2144, 2023. https://doi.org/10.1007/s00419-023-02376-6.

[23] A.A. Pasand, S.M. Zahrai, Seismic control of tall buildings using vertically distributed multiple tuned mass dampers, Structural Design of Tall and Special Buildings, 33(14), e2123, 2024. https://doi.org/10.1002/tal.2123.

[24] H.R. Rahmani, C. Könke, Seismic control of tall buildings using distributed multiple tuned mass dampers, Advances in Civil Engineering, 2019, 1–19. https://doi.org/10.1155/2019/6480384.

[25] L. Meirovitch (2001). Fundamentals of Vibrations. McGraw-Hill.

[26] A.K. Chopra, Dynamics of Structures: Theory and Applications to Earthquake Engineering, 4th ed., Pearson Education, 2012.

[27] R. W. Clough & J. Penzien, (2003). Dynamics of Structures (3rd ed.). Computers & Structures, Inc.

[28] J. Humar (2012). Dynamics of Structures (3rd ed.). CRC Press.

[29] S. Vasilopoulos, K. McTavish, A. Elshaer, Governing lateral load on tall buildings in Canadian regions, Sustainability, 16(16), 6757, 2024. https://doi.org/10.3390/su16166757.

[30] D.J. Inman, Vibrations with Control, Measurement and Stability, John Wiley & Sons Ltd, New York, 2006.

[31] Quanser, Shake Table II – Bench-scale single-axis motion simulator, [Online], Available at: https://www.quanser.com/products/shake-table-ii/ (Accessed: 21 March 2025).

[32] G.C. Marano, R. Greco, B. Chiaia, A comparison between different optimization criteria for tuned mass dampers design, Journal of Sound and Vibration, 329(23), 4880–4890, 2010. [Online], Available at: https://doi.org/10.1016/j.jsv.2010.05.015

[33] M. Khazaei, R. Vahdani, A. Kheyroddin, Optimal location of multiple tuned mass dampers in regular and irregular tall steel buildings plan, Shock and Vibration, 2020, Article ID 9072637. Available at: https://doi.org/10.1155/2020/9072637

[34] M. De Angelis, M. Basili, D. Pietrosanti, On the optimal design and placement of Tuned-Mass-Damper-Inerter for Multi-Degree-Of-Freedom structures, Structures, 56, 104781, October 2023. Available at: https://doi.org/10.1016/j.istruc.2023.06.112

[35] Pacific Earthquake Engineering Research Center (PEER), OpenSees – Open System for Earthquake Engineering Simulation, [Online], Available at: https://opensees.berkeley.edu/ (Accessed: 21 March 2025).